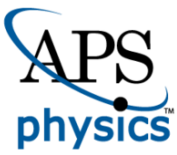

Dirac Line Nodes in Inversion-Symmetric Crystals

Youngkuk Kim, Benjamin J. Wieder, C. L. Kane, and Andrew M. Rappe

Phys. Rev. Lett. **115**, 036806 — Published 17 July 2015

DOI: 10.1103/PhysRevLett.115.036806

Dirac Line Nodes in Inversion Symmetric Crystals

Youngkuk Kim,[1] Benjamin J. Wieder,[2] C. L. Kane,[2] and Andrew M. Rappe[1]

[1] *The Makineni Theoretical Laboratories, Department of Chemistry, University of Pennsylvania, Philadelphia, Pennsylvania 19104–6323, USA*

[2] *Department of Physics and Astronomy, University of Pennsylvania, Philadelphia, Pennsylvania 19104–6396, USA*

(Dated: June 8, 2015)

We propose and characterize a new $\mathbb{Z}_2$ class of topological semimetals with a vanishing spin–orbit interaction. The proposed topological semimetals are characterized by the presence of bulk one-dimensional (1D) Dirac Line Nodes (DLNs) and two-dimensional (2D) nearly-flat surface states, protected by inversion and time–reversal symmetries. We develop the $\mathbb{Z}_2$ invariants dictating the presence of DLNs based on parity eigenvalues at the parity–invariant points in reciprocal space. Moreover, using first-principles calculations, we predict DLNs to occur in Cu_3N near the Fermi energy by doping non-magnetic transition metal atoms, such as Zn and Pd, with the 2D surface states emerging in the projected interior of the DLNs. This paper includes a brief discussion of the effects of spin–orbit interactions and symmetry-breaking as well as comments on experimental implications.

A recent development in condensed matter physics has been the discovery of semimetallic features in electronic band structures protected by the interplay of symmetry and topology. A tremendous amount of progress has been made in materials with strong spin–orbit interactions, such as the surface states of topological insulators [1, 2] and topological crystalline insulators [3], as well as the gapless bulk states of Weyl and Dirac semimetals [4–6]. Related topological phenomena can occur in materials with vanishing (or weak) spin–orbit interactions [7]. Indeed, the prototypical topological semimetal is graphene [8], which exhibits Dirac points that are robust to the extent that the spin–orbit interaction in carbon is weak. In the absence of spin–orbit interactions, the Dirac points in graphene are topologically protected by the combination of inversion and time–reversal symmetries.

In this paper we study a related phenomenon for three dimensional (3D) materials with weak spin–orbit interaction. We show that the combination of inversion and time–reversal symmetries protects Dirac line nodes (DLNs), for which the conduction band and valence band meet along a line in momentum space, and we predict realistic materials in which they should occur. DLNs have been discussed previously in the context of models that have an additional chiral symmetry [9, 10], which can arise on a bipartite lattice with only nearest neighbor hopping. In this case, the DLN can be constrained to occur at zero energy [11]. However, chiral symmetry is never expected to be an exact symmetry of a band structure. We will show that despite the absence of chiral symmetry, the line node is protected, though it is not constrained to sit at a constant energy. We will show, however, that in the vicinity of a band inversion transition, a DLN can occur in the form of a small circle, whose energy is approximately flat. The presence of such a Dirac circle has interesting consequences for the surface states, and we show that on the projected interior of the Dirac circle, the surface exhibits a nearly flat band, which must be half–filled when the surface is electrically neutral. Such surface states could be an interesting platform for strong correlation physics [12]. We introduce a class of materials and use first–principles density functional theory (DFT) calculations to show that they can be tuned through the band inversion transition and exhibit the predicted Dirac circle, as well as a more complex nodal structure. A similar DLN has recently been predicted in graphite [13, 14], a hyper-honeycomb lattice [15], and 3D carbon allotropes [16, 17]. Recently, DLNs also have been proposed in systems, with strong spin-orbit interactions, such as perovskite irridates [18, 19] and non-centrosymetric semimetals [20], but in those systems the mechanism of symmetry protection is different.

We will begin by elucidating the topological constraints that inversion and time–reversal symmetries impose. We will then introduce a $\mathbb{Z}_2$ topological invariant (related to the invariant characterizing a 3D topological insulator) which signifies the presence of DLNs. We will then present DFT calculations on transition metal–doped Cu_3N that predict a Dirac circle, as well as nearly-flat boundary modes. We will then introduce a simple low–energy $k \cdot p$ model that explains the appearance of the Dirac circle at a band inversion, and allows for a simple description of the resulting boundary modes.

Consider a 3D Bloch Hamiltonian $\mathcal{H}(\mathbf{k})$ that is invariant under inversion $\mathcal{P}$ and time–reversal $\mathcal{T}$. In the absence of spin–orbit interactions we may consider $\mathcal{T}^2 = +1$. The occupied Bloch eigenstates are characterized by a Berry connection $\mathbf{A}(\mathbf{k}) = -i\sum_n \langle u_n(\mathbf{k})|\nabla_{\mathbf{k}} u_n(\mathbf{k})\rangle$. $\mathcal{P}$ and $\mathcal{T}$ symmetries constrain the Berry phase, $\omega(C) = \exp i \oint_C \mathbf{A}\cdot d\mathbf{k}$, on any closed loop C in momentum space, to satisfy $\omega(C) = \omega(-C)$ and $\omega(C) = \omega(-C)^*$, respectively. It follows that loops C are characterized by a $\mathbb{Z}_2$ topological invariant $\omega(C) = \pm 1$ [21]. The non–trivial loops $\omega(C) = -1$ must enclose a degeneracy. In two dimensions, this explains the symmetry protection of the Dirac points in graphene. In three dimensions, it guar-

antees that a line of degeneracies must pierce any surface bounded by C.

The parity eigenvalues $\xi_n(\Gamma_a) = \pm 1$ of the occupied Bloch states at the 8 parity–invariant momenta Γ_a provide an important constraint that allows us to identify topologically protected line nodes. First, consider a time-reversal invariant loop $C_{ab} = c_{ab} - \bar{c}_{ab}$ that connects Γ_a and Γ_b along two time–reversed paths c_{ab} and $\bar{c}_{ab}$. In the supplementary material we prove that the Berry phase on this loop satisfies

$$\omega(C_{ab}) = \xi_a \xi_b; \qquad \xi_a = \prod_n \xi_n(\Gamma_a). \tag{1}$$

If we now consider four parity-invariant points, the contour $C_{ab} - C_{cd}$ defines the boundary ∂S_{abcd} of a surface S_{abcd} in momentum space. The Berry phase on ∂S_{abcd} counts the number of DLNs $N(S_{abcd})$ that pierce that surface. We thus conclude that

$$(-1)^{N(S_{abcd})} = \xi_a \xi_b \xi_c \xi_d. \tag{2}$$

Thus, when $\xi_a \xi_b \xi_c \xi_d = -1$ there must be an odd number of DLN piercing any surface S_{abcd}, with the simplest case being just a single one. This relation is quite similar to the topological invariants $(\nu_0; \nu_1 \nu_2 \nu_3)$ characterizing a (strong or weak) $\mathbb{Z}_2$ topological insulator in the presence of spin–orbit interactions [22, 23]. Indeed, in a topological insulator with $\xi_a \xi_b \xi_c \xi_d = -1$, when the spin–orbit interaction is turned off a DLN must appear, because the system can not be adiabatically connected to a trivial insulator.

This connection to the parity eigenvalues suggests a route towards realizing the DLNs: Starting with a trivial insulator, invert a pair of opposite-parity bands. At the inversion transition a small Dirac circle will necessarily emerge and grow. In the following we will predict a class of real materials which exhibits this behavior, and analyze the low–energy structures which emerge.

Searching for materials that consist of light elements and preserve $\mathcal{T}$ and $\mathcal{P}$ symmetries, we find that copper nitride, Cu_3N, a narrow–gap semiconductor ($E_g \sim 0.3$ eV) [24], fosters DLNs near the Fermi level via an insulator–to–metal transition driven by doping transition metal atoms. Copper nitride, first synthesized in 1939 [24], is stable in air at room temperature with a cubic anti–ReO_3 structure in space group 221 ($Pm\bar{3}m$). It contains a rather large void at the center of the cubic unit cell, as shown in Fig. 1. This void can host extrinsic atoms such as N [25], Li [26, 27], Pd [28–32], Rh, Ru [32], Zn, Ni, Cd [28], Cu [27, 33], Fe, Ti [34], Ag [35], La, Ce [36], as well as many other transition–metal atoms [37]. In particular Ni, Cu, Pd, An, Ag, and Cd [28] are found to drive an electronic transition in Cu_3N into a semimetal without breaking $\mathcal{T}$ symmetry [37], by which we expect that DLNs form near the Fermi energy.

To demonstrate the existence of DLNs in the transition metal–doped Cu_3N, we perform first–principles calculations based on DFT. We employ the Perdew–Burke–Ernzerhof–type generalized gradient approximation [38] as implemented in the QUANTUM ESPRESSO package [39]. Norm–conserving, optimized, designed nonlocal pseudopotentials are generated by the OPIUM package [40, 41]. The wave functions are expanded in a plane–wave basis with an energy cutoff of 680 eV. We initially consider the spin–orbit interaction based on a scalar–relativistic pseudopotential [42], and later, we will discuss the effect of spin–orbit interactions, based on a fully-relativistic non–collinear scheme.

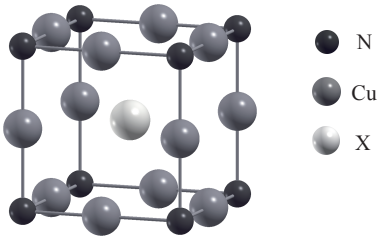

FIG. 1. Crystal structure of Cu_3NX. X represents a transition metal atom intercalated at the body–center of the cubic unit cell of Cu_3N in an anti–ReO_3 structure.

The low–energy electronic structures of Cu_3NX are more or less similar for X = {Ni, Cu, Pd, An, Ag, Cd}, as reported in Ref. [28]. Here we present the results of Cu_3NZn and Cu_3NPd as representatives of transition metal–doped Cu_3N systems. Note that these are extreme cases where the transition metal atoms are maximally doped [43]. In Cu_3NZn the conduction and valence bands are mainly comprised of conduction A_{2u} and valence A_{1g} states near the Fermi energy. As shown in Fig. 2, these bands are inverted at the X points, forming two–dimensional (2D) Dirac points on the X–M and R–X lines (enclosed by red circles in the figure). These Dirac points signal the presence of a DLN enclosing X. Although there are more degenerate points near the Fermi level, and bands crossing the Fermi energy near the R point, we will simplify and here focus only on the bands near X. On the other hand, the conduction and valence bands of Cu_3NPd are comprised of T_{2g} and T_{1u} states, which are inverted at the R point, forming the Dirac points on the R–X and M–R lines. These Dirac points are in fact parts of a DLN that encloses the R point, as shown below.

The nodal lines of the conduction and valence bands in the 3D BZ are shown in Fig. 3. As mentioned above, DLNs appear near the X points in the Cu_3NZn system. The cubic symmetry of the system dictates three DLNs encircling the three inequivalent X points $X^r = \pi \hat{r}/a$, where $r = x, y$, and z. Similarly, Cu_3NPd also exhibits three DLNs due to the cubic symmetry, but since they appear enclosing the R point, they form in a gyroscope shape. In both systems, the DLNs are contained in three mirror-invariant planes at X^x, X^y, and X^z, due to the

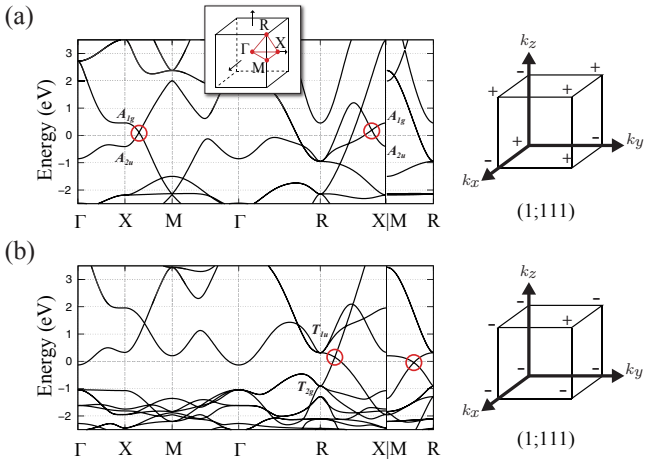

FIG. 2. (color online) Electronic structures and $\mathbb{Z}_2$ indices of (a) Cu_3NZn and (b) Cu_3NPd. Bands are drawn along the high–symmetry lines of the BZ (inset). The Dirac points are indicated by red circles. Parity eigenvalues are illustrated at the eight parity–invariant points in the first octant of the BZ.

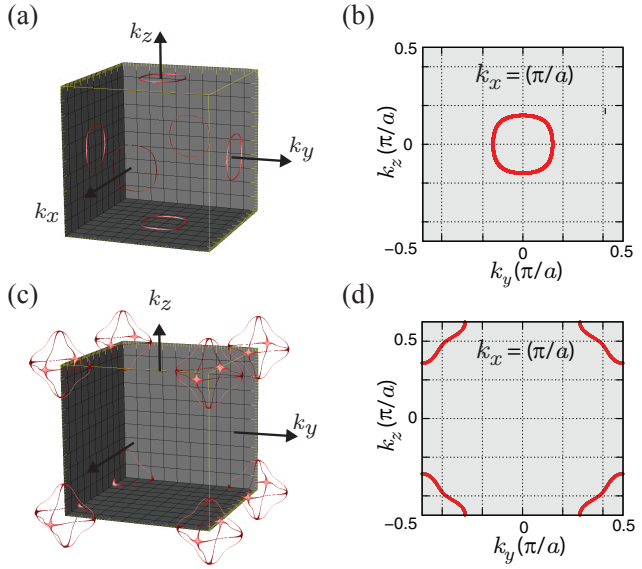

FIG. 3. (color online) Dirac line nodes in the Brillouin Zone (BZ). (a) and (b) Cu_3NZn, and (c) and (d) Cu_3NPd. The DLNs are illustrated by red curves in the 3D BZ [(a) and (c)] and on the 2D boundary plane of the BZ at $k = X^x$ [(b) and (d)].

corresponding mirror symmetries. We expect that breaking the mirror symmetries should unlock the DLNs from the mirror planes, but that the DLNs will survive as they are protected by $\mathcal{P}$ and $\mathcal{T}$.

The appearance of DLNs agrees with the topological prediction of $\mathbb{Z}_2$ invariants $(\nu_0;\nu_1\nu_2\nu_3)$, calculated from the parity analysis. In Cu_3NZn, parities at the eight time–reversal invariant momenta $(\Gamma, 3X, 3M, R)$ give $(\nu_0;\nu_1\nu_2\nu_3) = (1;111)$, which dictates that there should be DLNs threading half the invariant plane at $X^r = \pi\hat{r}/a$ $(r = x, y, z)$ an odd number of times. The three DLNs enclosing the X points fulfill this topological constraint (see the supplementary material for more details of this analysis). Similarly, in Cu_3NPd we find that $(\nu_0;\nu_1\nu_2\nu_3) = (1;111)$, which is also in accordance with the formation of the three DLNs enclosing R. In this case, each invariant plane at X^r is threaded three times by all three DLNs.

A low–energy $\boldsymbol{k}\cdot\boldsymbol{p}$ Hamiltonian describing the conduction A_{2u} and valence A_{1g} states, which form the DLNs in Cu_3NZn, captures the essential features of the DLNs. Near X^r, symmetries dictate a two–band Hamiltonian

$$\mathcal{H}_r = (\bar{\epsilon}+a_\perp|\boldsymbol{q}_\perp|^2+a_r q_r^2)\mathbb{I}_\tau+vq_r\tau^y+(\Delta\epsilon+b_\perp|\boldsymbol{q}_\perp|^2+b_r q_r^2)\tau^z, \quad (3)$$

where $\boldsymbol{q} = \boldsymbol{k} - X^r$, $\perp$ represents the normal components to $\hat{r}$, and the Pauli matrices $\{\mathbb{I}_\tau, \tau^i\}$ describe the A_{1g} and A_{2u} states. The form of $\mathcal{H}_r$ is uniquely determined by inversion $\mathcal{P} = \tau^z$ and time–reversal $\mathcal{T} = K$ (K being complex conjugation), together with the D_{4h} point group symmetries of X. It gives energy eigenvalues

$$E_\pm(\boldsymbol{q}) = \bar{\epsilon} + a_\perp|\boldsymbol{q}_\perp|^2 + a_r q_r^2 \pm \sqrt{(\Delta\epsilon + b_\perp|\boldsymbol{q}_\perp|^2 + b_r q_r^2)^2 + v^2 q_r^2}. \quad (4)$$

A DLN forms at $q_r = 0$ and $|\boldsymbol{q}_\perp|^2 \equiv q_0^2 = -\Delta/b_\perp$, when the bands are inverted ($\Delta\epsilon < 0$). The DFT results determine $\Delta\epsilon \sim -0.4$ eV. In Cu_3NPd, unlike in Cu_3NZn, there are conduction T_{2g} and valence T_{1u} states, instead leading to a six–band Hamiltonian $\mathcal{H}$. However, this can be decomposed into three copies of $\mathcal{H}_r$ with $r = x, y$, and z and $\mathcal{H} = \mathcal{H}_x \oplus \mathcal{H}_y \oplus \mathcal{H}_z$, giving rise to three gyroscope–shaped DLNs. Therefore, the essential features of the DLNs should be the same between Cu_3NZn and Cu_3NPd, aside from the former having a single DLN occurring in three inequivalent valleys of the BZ (X points) and the latter having three DLNs in a single valley (R point).

This model Hamiltonian also describes boundary modes. Consider a boundary perpendicular to $\hat{r}$ in which $\Delta\epsilon$ varies between a negative (inverted) value and a large positive value. Fixing $q_\perp$ and considering the theory to linear order in $q_r \to -i\partial_r$,

$$\mathcal{H}_z(\boldsymbol{q}) = -iv\tau^y\partial_r+(\Delta\epsilon(r)+b_\perp q_\perp^2)\tau^z+(\bar{\epsilon}+a_\perp q_\perp^2)\mathbb{I}_\tau. \quad (5)$$

For each $k_\perp$ this defines a Jackiw–Rebbi problem [44]. When $\Delta\epsilon + b_\perp k_\perp^2 < 0$ there will be a boundary mode at the surface. In general the boundary band is not flat, but disperses for $k_\perp < k_F$

$$\epsilon_0(k_\perp) = \bar{\epsilon} + a_\perp k_\perp^2 \leq 0. \quad (6)$$

If $a = 0$ however, the surface band is flat. This reflects an additional chiral symmetry $\{\mathcal{H}, \tau^x\} = 0$ at this point. In this model, the value of a is related to the difference of the effective masses of the A_{1g} and A_{2u} bands. If the surface in the absence of inversion is electrically neutral,

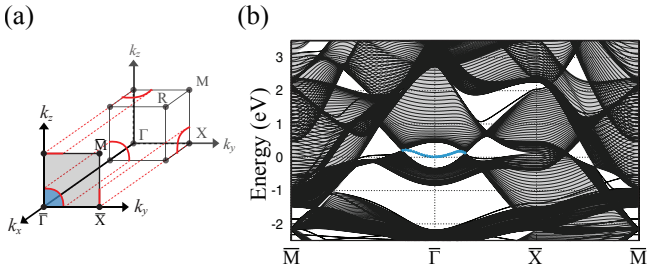

FIG. 4. (color online) Two–dimensional surface electronic structure for Cu_3NZn. (a) First octant of three–dimensional Brillouin zone (BZ) of Cu_3NZn projected onto the two–dimensional surface BZ of the (100) surface and (b) surface electronic band structure. The Dirac line nodes (DLNs) and the projected interior of DLNs are illustrated with the red and blue schemes, respectively. The slab bands are shown in black lines and surface states in the enclosed region are shown in blue lines. The shaded region represents bulk bands projected onto the BZ of the (100) surface along k_x .

then after inversion the surface will be neutral when the surface band is *half–filled*. This leads to a narrow surface band, where electron density $q_0^2/4\pi = |\Delta\epsilon|/4\pi b_\perp$ is controlled by the degree of band inversion. In the absence of screening from other bands, this surface band will tend to be pinned at the Fermi energy.

To study the surface states in Cu_3NZn, we calculate the band structures of a slab geometry with 40 unit cells, exposing the (100) Cu_2N surfaces to vacuum. Our calculation from first principles predicts that nearly-flat surface states emerge in the interiors of projected DLNs connecting the Dirac nodes, as shown in Fig. 4. The slab band structure exhibits the weakly-dispersing surface states near $\bar{\Gamma}$ in the projected interior of the DLN. The topological surface states resulting from closed DLNs are half–filled and nearly flat, providing a unique venue for interesting strong-correlation and transport physics.

The strong spin–orbit interaction can induce diverse topological phases in DLN semimetals, including topological insulators, 3D Dirac semimetals [5, 45, 46], or even other DLN semimetals [19]. Analogously to graphene, spin–orbit interaction can gap out DLNs and drive the system to a topologically-insulating phase. The resultant topological insulator should have the same topological $\mathbb{Z}_2$ indexes as the DLN semimetal from which it originated. More interestingly, an additional crystalline symmetry may protect a part of the DLN in a symmetry-invariant region of the BZ, resulting in topological Dirac semimetals or crystalline symmetry–protected DLNs with strong spin–orbit interactions. We have tested the effect of spin–orbit interaction in Cu_3NPd using a fully-relativistic non–collinear scheme, and indeed found that C_4 symmetry along the R–M line protects the Dirac point on the line, while the spin–orbit coupling otherwise opens a gap (with maximum size of ~ 62 meV on the R–X line), thus giving rise to a 3D Dirac semimetal phase in a strong spin–orbit interacting regime. Note that Cu_3NPd is an extreme case where Pd is maximally doped, and thus the spin–orbit interactions due to Pd $4d$ states are maximized. The spin–orbit interaction can be controlled either by the Pd–doping concentration, or by doping other group-X transition-metal atoms, such as Ni, Pd, and Pt. We thus expect both the DLN semimetal and 3D Dirac semimetal phases should be accessible in the Cu_3N system.

In summary, we have demonstrated that the combination of inversion and time–reversal symmetries allows for the $\mathbb{Z}_2$ classification of topological semimetals under vanishing spin–orbit interactions. The proposed topological semimetals are characterized by the presence of bulk DLNs and nearly-flat surface states, protected by inversion and time-reversal symmetries. Our first–principles calculations predict that the proposed topological phase can be observed in Cu_3N by doping with a class of nonmagnetic transition metal atoms X, where X = {Ni, Cu, Pd, Ag, Cd}. The 2D surface states predicted for the DLN semimetal can hopefully be experimentally observed through, for example, ARPES in Cu_3NX_x, using the doping concentration x as a knob to control the sizes of the closed DLN and the enclosed surface band. Doping with heavier atoms can also be used to potentially observe spin–orbit-induced topological phases.

While this manuscript was in the final stages of preparation we learned of recent work proposing DLN in Ca_3P_2 [47]. YK acknowledges support from NSF grant DMR–1120901. CLK acknowledges support from a Simons Investigator grant from the Simons Foundation. AMR acknowledge support from the DOE Office of Basic Energy Sciences, under grant number DE–FG02–07ER15920. Computational support is provided by the HPCMO of the U.S. DOD and the NERSC of the U.S. DOE.

[1] M. Z. Hasan and C. L. Kane, Rev. Mod. Phys. **82**, 3045 (2010).
[2] X.-L. Qi and S.-C. Zhang, Rev. Mod. Phys. **83**, 1057 (2011).
[3] L. Fu, Phys. Rev. Lett. **106**, 106802 (2011).
[4] X. Wan, A. M. Turner, A. Vishwanath, and S. Y. Savrasov, Phys. Rev. B **83**, 205101 (2011).
[5] S. M. Young, S. Zaheer, J. C. Y. Teo, C. L. Kane, E. J. Mele, and A. M. Rappe, Phys. Rev. Lett. **108**, 140405 (2012).
[6] J. A. Steinberg, S. M. Young, S. Zaheer, C. L. Kane, E. J. Mele, and A. M. Rappe, Phys. Rev. Lett. **112**, 036403 (2014).
[7] A. Alexandradinata, C. Fang, M. J. Gilbert, and B. A. Bernevig, Phys. Rev. Lett. **113**, 116403 (2014).
[8] Castro Neto, A. H. and Guinea, F. and Peres, N. M. R. and Novoselov, K. S. and Geim, A. K., Rev. Mod. Phys. **81**, 109 (2009).
[9] P. Hořava, Phys. Rev. Lett. **95**, 016405 (2005).

[10] A. P. Schnyder and S. Ryu, Phys. Rev. B **84**, 060504 (2011).
[11] S. Ryu and Y. Hatsugai, Phys. Rev. Lett. **89**, 077002 (2002).
[12] G. E. Volovik, arXiv:1110.4469.
[13] G. P. Mikitik and Y. V. Sharlai, Phys. Rev. B **73**, 235112 (2006).
[14] T. T. Heikkilä and G. E. Volovik, JETP Lett. **93**, 59 (2011).
[15] K. Mullen, B. Uchoa, and D. T. Glatzhofer, arXiv:1408.5522.
[16] H. Weng, Y. Liang, Q. Xu, Y. Rui, Z. Fang, X. Dai, and Y. Kawazoe, arXiv:1411.2175.
[17] Y. Chen, Y. Xie, S. A. Yang, H. Pan, F. Zhang, M. L. Cohen, and S. Zhang, arXiv:1505.02284.
[18] H.-S. Kim, Y. Chen, and H.-Y. Kee, arXiv:1411.1406.
[19] Y. Chen, Y.-M. Lu, and H.-Y. Kee, Nat. Commun. **6**, 6593 (2015).
[20] H. Weng, C. Fang, Z. Fang, B. A. Bernevig, and X. Dai, Phys. Rev. X **5**, 011029 (2015).
[21] Since $[\mathcal{H}(\mathbf{k}), \mathcal{PT}] = 0$, this $\mathcal{Z}_2$ invariant can also be understood as characterizing one parameter families of Hamiltonians in class AI [48].
[22] L. Fu, C. L. Kane, and E. J. Mele, Phys. Rev. Lett. **98**, 106803 (2007).
[23] L. Fu and C. L. Kane, Phys. Rev. B **76**, 045302 (2007).
[24] R. Juza and H. Hahn, Z. Anorg. Allg. Chem. **239**, 282 (1938).
[25] F. Hadian, A. Rahmati, H. Movla, and M. Khaksar, Vacuum **86**, 1067 (2012).
[26] F. Gulo, A. Simon, J. Khler, and R. K. Kremer, Angew. Chem. Int. Edit. **43**, 2032 (2004).
[27] Z. Hou, Solid State Sci. **10**, 1651 (2008).
[28] M. G. Moreno-Armenta, W. L. Prez, and N. Takeuchi, Solid State Sci. **9**, 166 (2007).
[29] U. Zachwieja and H. Jacobs, J. Less-Common Met. **161**, 175 (1990).
[30] U. Hahn and W. Weber, Phys. Rev. B **53**, 12684 (1996).
[31] A. Ji, C. Li, and Z. Cao, Appl. Phys. Lett. **89**, 252120 (2006).
[32] M. Sieberer, S. Khmelevskyi, and P. Mohn, Phys. Rev. B **74**, 014416 (2006).
[33] M. G. Moreno-Armenta, A. Martnez-Ruiz, and N. Takeuchi, Solid State Sci. **6**, 9 (2004).
[34] X. Fan, Z. Wu, G. Zhang, C. Li, B. Geng, H. Li, and P. Yan, J. Alloy. Compd. **440**, 254 (2007).
[35] J. Pierson and D. Horwat, Scripta Mater. **58**, 568 (2008).
[36] Z. Wu, H. Chen, N. Gao, E. Zhang, J. Yang, T. Yang, X. Li, and W. Huang, Comp. Mater. Sci. **95**, 221 (2014).
[37] X. Cui, A. Soon, A. Phillips, R. Zheng, Z. Liu, B. Delley, S. Ringer, and C. Stampfl, J. Magn. Magn. Mater. **324**, 3138 (2012).
[38] J. P. Perdew, K. Burke, and M. Ernzerhof, Phys. Rev. Lett. **77**, 3865 (1996).
[39] P. Giannozzi *et al.*, J. Phys. Condens. Mat. **21**, 395502 (2009).
[40] A. M. Rappe, K. M. Rabe, E. Kaxiras, and J. D. Joannopoulos, Phys. Rev. B **41**, 1227 (1990).
[41] N. J. Ramer and A. M. Rappe, Phys. Rev. B **59**, 12471 (1999).
[42] I. Grinberg, N. J. Ramer, and A. M. Rappe, Phys. Rev. B **62**, 2311 (2000).
[43] See supplementary material at http://link.aps.org/supplemental/10.1103/PhysRevLett.111.180001 for the discussion on the doping concentration.
[44] R. Jackiw and C. Rebbi, Phys. Rev. D **13**, 3398 (1976).
[45] Z. Wang, Y. Sun, X.-Q. Chen, C. Franchini, G. Xu, H. Weng, X. Dai, and Z. Fang, Phys. Rev. B **85**, 195320 (2012).
[46] Z. Wang, H. Weng, Q. Wu, X. Dai, and Z. Fang, Phys. Rev. B **88**, 125427 (2013).
[47] L. S. Xie, L. M. Schoop, E. M. Seibel, Q. D. Gibson, W. Xie, and R. J. Cava, arXiv:1504.01731.
[48] J. C. Y. Teo and C. L. Kane, Phys. Rev. B **82**, 115120 (2010).